The International Journal of Biochemistry & Cell Biology 76 (2016) 19–30

Contents lists available at ScienceDirect

The International Journal of Biochemistry & Cell Biology

journal homepage: www.elsevier.com/locate/biocel

Positive allosteric modulators of α7 nicotinic acetylcholine receptors affect neither the function of other ligand- and voltage-gated ion channels and acetylcholinesterase, nor β-amyloid content

Hugo R. Arias[a,*], Federica Ravazzini[b], Katarzyna M. Targowska-Duda[c], Agnieszka A. Kaczor[d,e], Dominik Feuerbach[f], Juan C. Boffi[g], Piotr Draczkowski[d], Dirk Montag[h], Brandon M. Brown[i], Ana Belén Elgoyhen[g], Krzysztof Jozwiak[c], Giulia Puia[b]

[a] Department of Medical Education, California Northstate University College of Medicine, Elk Grove, CA, USA
[b] Department of Life Science, University of Modena and Reggio Emilia, Modena, Italy
[c] Department of Biopharmacy, Medical University of Lublin, Lublin, Poland
[d] Department of Synthesis and Chemical Technology of Pharmaceutical Substances with Computer Modeling Lab, Medical University of Lublin, Lublin, Poland
[e] Department of Pharmaceutical Chemistry, School of Pharmacy, University of Eastern Finland, Kuopio, Finland
[f] Novartis Institutes for Biomedical Research, Basel, Switzerland
[g] Instituto de Investigaciones en Ingeniería Genética y Biología Molecular, Dr. Héctor N. Torres, CONICET, Buenos Aires, Argentina
[h] Neurogenetics Special Laboratory, Leibniz Institute for Neurobiology, Magdeburg, Germany
[i] Department of Pharmacology, University of California, Davis, CA, USA

ARTICLE INFO

Article history:
Received 23 March 2016
Received in revised form 22 April 2016
Accepted 25 April 2016
Available online 26 April 2016

Keywords:
α7 Nicotinic acetylcholine receptor positive allosteric modulators
Serotonin type 3 and glutamate receptors
Acetylcholinesterase
β-Amyloid
Molecular docking and molecular dynamics

ABSTRACT

The activity of positive allosteric modulators (PAMs) of α7 nicotinic acetylcholine receptors (AChRs), including 3-furan-2-yl-*N*-*p*-tolyl-acrylamide (PAM-2), 3-furan-2-yl-*N*-*o*-tolylacrylamide (PAM-3), and 3-furan-2-yl-*N*-phenylacrylamide (PAM-4), was tested on a variety of ligand- [i.e., human (h) α7, rat (r) α9α10, hα3-containing AChRs, mouse (m) 5-HT_{3A}R, and several glutamate receptors (GluRs)] and voltage-gated (i.e., sodium and potassium) ion channels, as well as on acetylcholinesterase (AChE) and β-amyloid (Aβ) content. The functional results indicate that PAM-2 inhibits hα3-containing AChRs (IC_{50} = 26 ± 6 μM) with higher potency than that for NR1aNR2B and NR1aNR2A, two NMDA-sensitive GluRs. PAM-2 affects neither the activity of m5-HT_{3A}Rs, GluR5/KA2 (a kainate-sensitive GluR), nor AChE, and PAM-4 does not affect agonist-activated rα9α10 AChRs. Relevant clinical concentrations of PAM-2–4 do not inhibit Na_v1.2 and K_v3.1 ion channels. These PAMs slightly enhance the activity of GluR1 and GluR2, two AMPA-sensitive GluRs. PAM-2 does not change the levels of $A_{β42}$ in an Alzheimer's disease mouse model (i.e., 5XFAD). The molecular docking and dynamics results using the hα7 model suggest that the active sites for PAM-2 include the intrasubunit (i.e., PNU-120596 locus) and intersubunit sites. These results support our previous study showing that these PAMs are selective for the α7 AChR, and clarify that the procognitive/promnesic/antidepressant activity of PAM-2 is not mediated by other targets.
© 2016 Elsevier Ltd. All rights reserved.

Abbreviations: 5-HT, 5-hydroxytryptamine (serotonin); m5-HT3AR, murine serotonin type 3A receptor; AChR, nicotinic acetylcholine receptor; ACh, acetylcholine; NMDAR, *N*-methyl-*D*-aspartate receptor; AMPAR, α-amino-3-hydroxy-5-methyl-4-isoxazolepropionic acid receptor; NIC, nicotine; MLA, methyllycaconitine; ACTh, acetyltiocholine; AChE, acetylcholinesterase; ECD, extracellular domain; TMD, transmembrane domain; PAM, positive allosteric modulator; PAM-2, 3-furan-2-yl-*N*-*p*-tolyl-acrylamide; PAM-3, 3-furan-2-yl-*N*-*o*-tolylacrylamide; PAM-4, 3-furan-2-yl-*N*-phenylacrylamide; AMPA, α-amino-3-hydroxy-5-methyl-4-isoxazolepropionic acid; NMDA, *N*-methyl-*D*-aspartic acid; KA, kainate; Nav1.2, voltage-gated sodium channel type 1.2; Kv3.1, voltage-gated potassium channel type 3.1; RT, room temperature; Vmax, maximum rate of enzymatic reaction; Km, Michaelis constant; IC50, ligand concentration that produces 50% inhibition; Ki, inhibition constant; nH, Hill coefficient; DMEM, Dulbecco's Modified Eagle Medium; FBS, fetal bovine serum.

* Corresponding author.
E-mail address: hugo.arias@cnsu.edu (H.R. Arias).

http://dx.doi.org/10.1016/j.biocel.2016.04.015
1357-2725/© 2016 Elsevier Ltd. All rights reserved.

1. Introduction

In recent years, many agonists, antagonists, and positive allosteric modulators (PAMs) with selectivity for the α7 nicotinic acetylcholine receptor (AChR) have been recently studied as potential treatments for different neurological disorders (reviewed in Arias, 2010; Malysz et al., 2009; Chatzidaki and Millar, 2015). In particular, PAMs have generated a lot of expectation since these compounds can potentiate the α7 AChR activity elicited by endogenous neurotransmitters, ACh and choline, potentially producing fewer side effects than exogenous agonists. In previous studies, the activity of three α7-PAMs (PAM-2–4) was characterized (Arias et al., 2011; Targowska-Duda et al., 2014; Andersen et al., 2016). These PAMs enhance agonist-induced α7 AChR activity (Arias et al., 2011) and reactivate desensitized α7 AChRs (Targowska-Duda et al., 2014) supporting a type II PAM classification. Additional microscopic current results showed that these PAMs behave as type I PAM at 22 °C, whereas this activity decreased at higher temperatures (i.e., 34 °C), coincident with type II PAMs (Andersen et al., 2016). In conclusion, PAM-2–4, present pharmacological properties of both type I and type II PAMs, that make them different to other α7 PAMs.

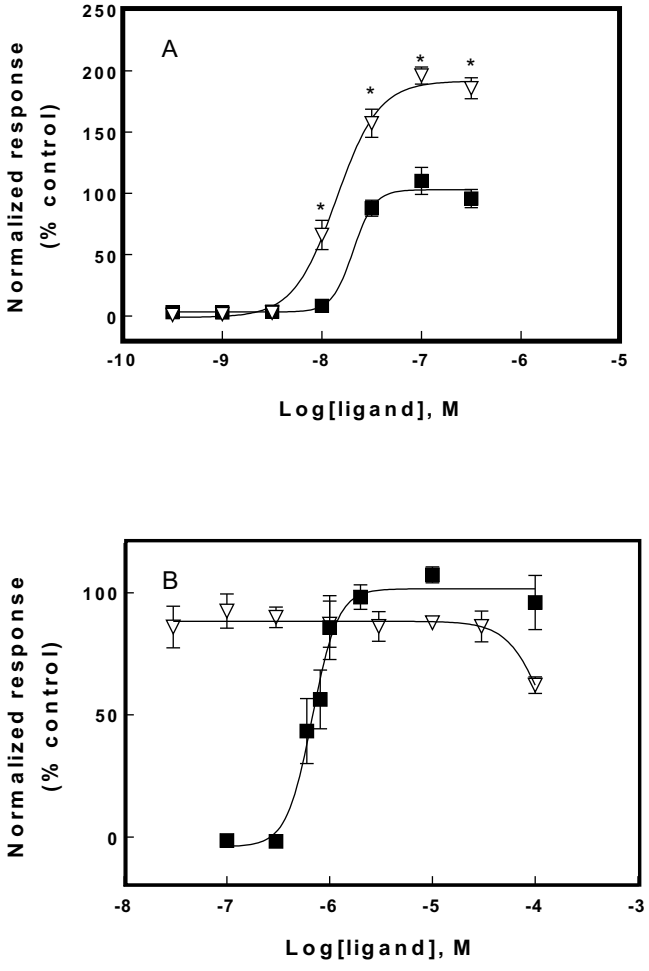

Fig. 1. Effect of PAM-2 on agonist-induced Ca^{2+} influx in CH3-hα7 and N1E115-m5-HT_3 cells. (A) Increased concentrations of (±)-epibatidine (■) activate hα7 AChRs with potency EC_{50} = 52 ± 4 nM (n = 28). PAM-2 (10 μM) (▽) increases (±)-epibatidine-induced hα7 AChR activity with apparent EC_{50} = 17 ± 5 nM and E_{max} = 190 ± 5% (n = 3). Statistical analysis was performed by a paired *t*-test with Sidak-Bonferroni correction for repeated measurements. The results indicated that both curves are different (P < 0.02) in the concentration range labeled with *. (B) Increased concentrations of 5-HT (■) activate m5-HT_3Rs with EC_{50} = 0.55 ± 0.03 μM (n = 47). Subsequently, cells were pre-treated with several concentrations of PAM-2 (▽) followed by addition of 1 μM 5-HT (n = 3). Agonist responses were normalized to the maximal response which was set as 100%. Each data point is the mean ± SEM. The apparent EC_{50}, E_{max}, and n_H values are summarized in Table 1.

To complete the initial studies on receptor selectivity performed on several human (h) AChR subtypes (Arias et al., 2011, 2015a), the activity of PAM-2 was tested on other members of the Cys-loop family, including rat (r)α9α10 and hα3-containing AChRs as well as mouse (m)5-HT_{3A}Rs. We also determined whether PAM-2 can modulate choline-evoked α7 nAChR currents when low concentrations of choline are used.

Since PAM-2 has procognitive (Potasiewicz et al., 2015) and promnesic (Targowska-Duda et al., 2016) activities, and glutamate receptors (GluRs) are important for learning and memory processes (Gécz, 2010; Collingridge et al., 2013), the activity of PAM-2 was determined on several GluR subtypes, including those sensitive to *N*-methyl-D-aspartate (NMDA) (i.e., hNR1aNR2A and hNR1aNR2B), α-amino-3-hydroxy-5-methyl-4-isoxazolepropionic acid (AMPA) (i.e., GluR1 and GluR2), and kainate (KA) (i.e., GluR5/KA2).

Since $Na_v1.2$ (Ahn et al., 2007) and $K_v3.1$ (Perney et al., 1992) channels are found in the hippocampus, and this brain area is considered very important for cognitive and memory functions, the activity of these PAMs was tested on these channels.

Taking into account that some acetylcholinesterase (AChE) inhibitors used in the treatment of Alzheimer's disease (i.e., tacrine and galantamine) are also PAMs at different AChRs (Storch et al., 1995; reviewed in Arias, 2010, 2011), the activity of PAM-2 was also tested on the AChE. Since the chronic application of galantamine reduces the plaque density in 5XFAD transgenic mice (Bhattacharya et al., 2014), an Alzheimer's disease animal model (Oakley et al., 2006), the effect of PAM-2 on brain levels of $A_{\beta 42}$ (i.e., active species) was also determined in the same transgenic mice.

Our previous molecular docking results suggest that PAM-2–4 may bind to either the extracellular domain (ECD), transmembrane domain (TMD), and/or the ECD-TMD junction (Arias et al., 2011). To determine what domain is the most important, PAM-2 activity was correlated with the structural components (i.e., determined by molecular docking and molecular dynamics) of the binding sites at the hα7 AChR and mouse (m)5-HT_{3A}Rs. Based on our study, PAM-2–4 are selective for the hα7 AChR, where they bind to the TMD at the intrasubunit (i.e., the PNU-120596 locus) and intersubunit sites.

2. Material and methods

2.1. Materials

(±)-Epibatidine hydrochloride and serotonin hydrochloride (5-HT) were obtained from Tocris Bioscience (Ellisville, Missouri, USA). Fetal bovine serum (FBS) and trypsin/EDTA were purchased form Gibco BRL (Paisley, UK). Acetylthiocholine (ACTh), 5,5′-dithiobis(2-nitrobenzoic acid) (DTNB), acetylcholinesterase from *Electrophorus electricus*, poly-ornithine coated 24-well dishes, methyllycaconitine (MLA), (−)-nicotine hemisulfate (NIC), *N*-methyl-D-aspartic acid (NMDA), α-amino-3-hydroxy-5-methyl-4-isoxazolepropionic acid (AMPA), kainate (KA), glycine hydrochloride, choline chloride, PEG200, and acetylcholine chloride (ACh) were obtained from Sigma-Aldrich (St. Louis, MO, USA), whereas probenecid was obtained from Sigma-Aldrich (Buchs, Switzerland). Trypsin–EDTA was obtained from Euroclone (Milan, Italy). Dulbecco's Modified Eagle Medium (DMEM) was obtained from Seromed (Biochrom, Berlin, Germany), and Fluo-4 was purchased from Molecular Probes (Eugene, Oregon, USA). PAM-2–4 were synthesized as described previously (Arias et al., 2011). Salts, solvents, and reagents were purchased from commercial suppliers and used as received.

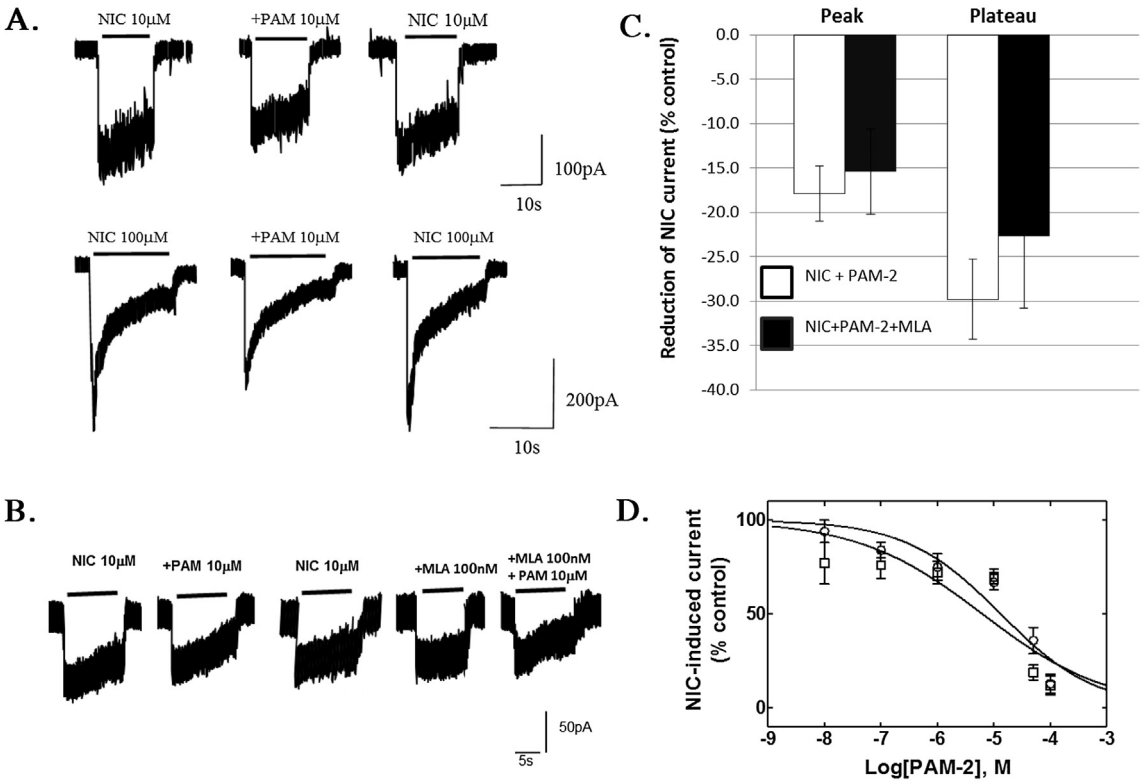

Fig. 2. PAM-2-induced inhibition of nicotine(NIC)-evoked currents in SH-SY5Y cells. (A) Representative electrophysiological recordings showing the effect of PAM-2 on the current evoked by 10 and 100 μM NIC, respectively. The bars (—) indicate the duration of the drug application. (B) Effect of 10 μM PAM-2 on NIC-evoked currents in the absence and the presence of 0.1 μM MLA. (C) Histogram showing the effect of PAM-2 (10 μM) on the peak and plateau currents evoked by 10 μM NIC in the absence and the presence of 0.1 μM MLA. Plateau currents are measured when the currents reach a steady value. Each data point is the mean ± SEM for 4–5 cells. No statistical differences were detected between the effect of PAM-2 with or without MLA (*t*-test; $P > 0.05$). (D) Concentration-response curves for PAM-2 on SH-SY5Y-AChRs activated by either 10 μM (○) or 100 μM (□) NIC. Each data point is the mean ± SEM for at least 6 cells. The obtained r^2 values are 0.92 (○) and 0.81 (□). The calculated IC_{50} and n_H values are summarized in Table 1.

2.2. Ca^{2+} influx measurements using the CH3-ha7 and N1E115-m5-HT3A cell lines

The CH3-ha7 (Arias et al., 2011) and N1E115-m5-HT_{3A} (Hussy et al., 1994) cells were cultured as described previously. The Ca^{2+} influx experiments using the CH3-ha7 cells are described elsewhere (Arias et al., 2011). On the day of the experiment, the medium was removed by flicking the plates and replaced with 100 μL DMEM (3.7 g/L $NaHCO_3$; 1.0 g/L glucose; with stable glutamine) supplemented with 10% (v/v) FBS, containing 2 μM Fluo-4 and 2.5 mM probenecid. The cells were then incubated at 37 °C in a humidified atmosphere (5% CO_2/95% air) for 1 h. Plates were flicked to remove excess of Fluo-4, cells washed once with HBSS buffer (130 mM NaCl, 4.5 mM KCl, 2 mM $CaCl_2$, 0.8 mM $MgSO_4$, 0.9 mM NaH_2PO_4, 25 mM glucose, 20 mM HEPES, pH 7.4). The N1E115-m5-HT_{3A} cell plates were refilled (100 μL) with different concentrations of PAM-2 and incubated for 5 min at RT. Plates were then placed in the cell plate stage of the fluorimetric imaging plate reader (Molecular Devices, Sunnyvale, CA, USA). A baseline consisting of 5 measurements of 0.4 s each was recorded. Agonists (i.e., 1 μM 5-HT to the N1E115-m5-HT_{3A} cells, and different concentrations of (±)-epibatidine to the GH3-hα7 cells) were then added to the cell plate using the 96-tip pipettor simultaneously to fluorescence recordings for 3 min. The laser excitation and emission wavelengths are 488 and 510 nm, at 1 W, with a CCD camera opening of 0.4 s. The potentiating EC_{50} and n_H values were determined by nonlinear regression.

2.3. Patch-clamp experiments using the SH-SY5Y, SH-SY5Y-hα7, JM4C, and HEK293 cell lines

The human neuroblastoma SH-SY5Y cells (Dunckley and Lukas, 2006), the SH-SY5Y-hα7 cells overexpressing the hα7 AChR (Arias et al., 2011), and the JM4C fibroblasts (kindly provided by Dr. Whiting) stably expressing the hNR1a and hNR2A or hNR1a and hNR2B subunits were cultured as previously described (Losi et al., 2008). HEK293 cells were transiently transfected with the respective GluR1, GluR2, GluR5, and GluR/K2 plasmids (generous gifts from Prof. Seeburg). For the electrophysiological experiments, cells were plated on glass coverslips in 35 mm dishes.

Patch-clamp recordings were performed at RT in the whole-cell configuration. During the experiments the cells were continuously perfused at 5 mL/min with standard solution containing: 145 mM NaCl, 5 mM KCl, 1 mM $CaCl_2$, 5 mM HEPES, 5 mM glucose, and 20 mM sucrose, pH 7.4. Patch electrodes had a resistance of 3–5 MΩ, and were filled with 140 mM KCl, 5 mM HEPES, 5 mM EGTA, 3 mM $MgCl_2$, and 2 mM Na_2ATP, pH 7.2. Cells were clamped at −60 mV and access resistance was monitored throughout the recordings. Currents were amplified with an Axopatch 1D amplifier, filtered at 5 kHz, digitized at 10 kHz. Drug application has a fast onset and achieves complete local perfusion (Y-tube system) of the recorded cell. Off-line data analysis and curve fitting were performed with pClamp 8 (Axon Instruments, Foster City, CA, USA).

The modulatory effect of PAM-2 was measured following this protocol: first, application of the agonist (choline, NMDA, Glu, or KA), and after 1 min, application of the agonist together with PAM-2

(at different concentrations). After 1–2 min of washout, the agonist was applied to check the complete recovery of the receptor.

2.4. Patch-clamp experiments using the neuroblastoma N1E115 and L929 cells expressing the respective $Na_v1.2$ and $K_v3.1$ ion channels

Experiments were conducted either manually with an EPC-10 amplifier (HEKA, Lambrecht/Pfalz, Germany) or on a QPatch-16 automated electrophysiology platform (Sophion Biosciences, Denmark). $K_v3.1$ expressing L292 cells were cultured as previously described (Grissmer et al., 1994), and subsequently trypsinized, plated onto poly-L-lysine coated coverslips and typically recorded 20–240 min after plating. $K_v3.1$ currents were elicited by 200-ms depolarizing pulses to 40 mV applied every 10 s (Schmitz et al., 2005) and recorded in normal Ringer solution [in mM: 160 NaCl, 4.5 KCl, 1 $MgCl_2$, 2$CaCl_2$ and 10HEPES; pH 7.4 (310 mOsm) with pipette solution containing 145 KF, 10HEPES, 10 EGTA, 2 $MgCl_2$, pH 7.2 (300 mOsm)].

Neuroblastoma N1E115 cells expressing $Na_v1.2$ channels were grown to ~70% confluency, rinsed in sterile PBS containing 0.02% EDTA, and lifted with 2 mL of TrypLE™ Express (Gibco, Grand Island, NY, USA) for ~2 min. Cells were dislodged by gentle tapping, suspended in DMEM, centrifuged and resuspended in 1 mL of external solution, placed into the Qfuge tube and resuspended in 150–200 μL extracellular solution after one additional spin on the QPatch. Whole-cell patch-clamp experiments were then carried out using disposable 16-channel planar patch chip plates (QPlates; patch hole diameter approximately 1 μm, resistance 2.00 ± 0.02 MΩ). Parameters were set as follows: positioning pressure −70 mbar, resistance increase for success 750%, minimum seal resistance 0.1 GΩ, holding potential −80 mV, holding pressure −20 mbar. $Na_v1.2$ were recorded with 20-ms pulses from −90 mV to 0 mV every 10 s with a KF-based internal solution and normal Ringer as an external solution.

2.5. Voltage-clamp experiments in oocytes

Xenopus laevis oocytes were injected with rat α9 and α10 subunit cRNAs (Verbitsky et al., 2000). Electrophysiological recordings were performed 2–6 days after cRNA injection under two-electrode voltage clamp with an Oocyte Clamp OC-725B or C amplifier (Warner Instruments Corp., Hamden, CT, USA), under the experimental conditions described previously (Elgoyhen et al., 2001). During electrophysiological recordings, oocytes were continuously superfused (~10 mL/min) with normal frog saline (115 mM NaCl, 2.5 mM KCl, 1.8 mM $CaCl_2$, and 10 mM HEPES buffer, pH 7.2). The membrane potential was clamped to −70 mV.

2.6. Effect of PAM-2 on AChE activity

The effect of PAM-2 on the activity of the *Electrophorus electricus* AChE was estimated by examining its influence on the AChE kinetics parameters (Ellman et al., 1961). The effect of 100 μM PAM-2 on the activity of AChE (~0.016 U) was estimated by a spectrophotometric method using the BioTec ELx800 Absorbance Microplate Reader (Winooski, VT, USA). After adding increasing concentrations of acetylthiocholine (ACTh) (in water), the absorbance at 450 nm is determined every 12-s for 10 min. The slopes of the obtained curves indicating the rate of enzymatic hydrolysis of the substrate (i.e., nmol of ACTh/min), in the absence and in the presence of PAM-2, were plotted against the used ACTh concentrations, and the respective K_m (Michaelis-Menten constant) and V_{max} (maximum rate) values were determined by nonlinear regression of the Michaelis-Menten model (Ellman et al., 1961).

2.7. Effect of PAM-2 on β-amyloid content

5XFAD transgenic male mice, overexpressing human $A_{β42}$ in the brain (Oakley et al., 2006), were obtained from The Jackson Laboratory (Bar Harbor, ME, USA) and subsequently crossed with B6SJLF1/J female mice. The resulting F2-offspring were used in all experiments. Transgenic mice were identified by PCR according to the supplier's protocol.

Male (n = 10) and female (n = 17) mice (5 months old) were intraperitoneally (i.p.) injected with either 2 mg/kg PAM-2 (n = 12) or vehicle (n = 15) (10% ethanol, 20% PEG200 in H_2O) for 26 consecutive days. At day 26, freshly harvested brain tissue was snapfrozen in liquid nitrogen and stored at −80 °C. $A_{β42}$ content was quantified in whole brain hemispheres by ELISA against human $A_{β42}$ (Thermo Fisher Scientific, Germany). For total $A_{β42}$ quantification, brains were homogenized in 5 M guanidine hydrochloride buffer (pH 8.0) and incubated for 4 h at RT. ELISA was then performed according to the manufacturer's instructions. Statview (SAS Institute Inc., Cary, NC, USA) was used for 2-way ANOVA (i.e., factors treatment and sex) and post-hoc analysis (Fisher PLSD). $P < 0.05$ values are considered significantly different.

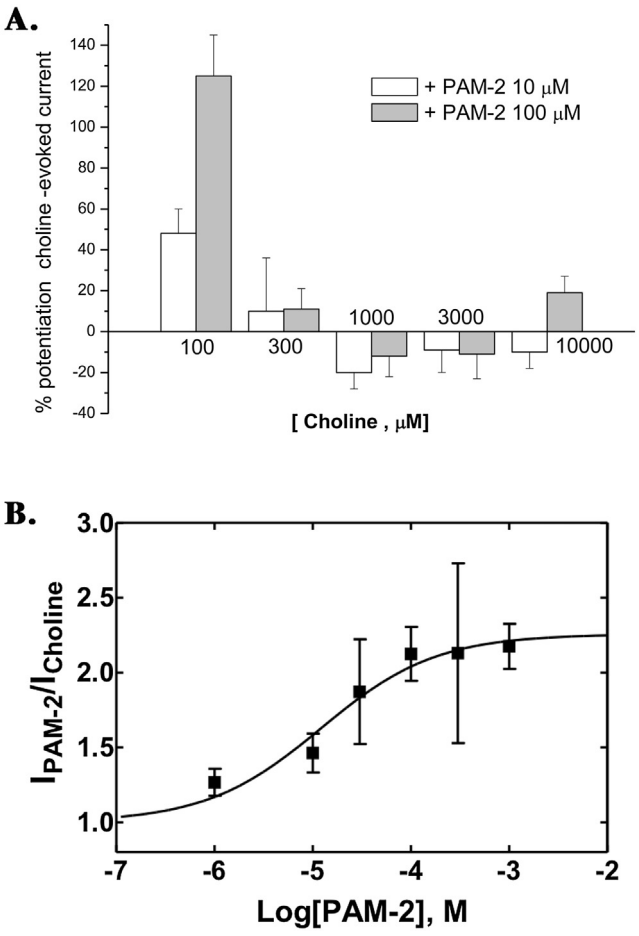

Fig. 3. PAM-2-induced modulation of choline-evoked currents in SH-SY5Y-hα7 cells. (A) Histograms showing the effect of 10 and 100 μM PAM-2 on hα7 AChR currents (% control) evoked by increasing concentrations of choline (i.e., 0.1–10 mM). Each data point is the mean ± SEM from 8 to 10 cells. (B) Concentration response curve for PAM-2 on hα7 AChR currents evoked by 100 μM choline. Each data point is the mean ± SEM from 4 to 13 experiments. The obtained r^2 value is 0.97.

2.8. Homology modeling, molecular docking, and molecular dynamics

The amino acid sequence and numbering of the hα7 subunit was obtained from the ExPASy Molecular Biology Server (http://www.us.expasy.org) (Gasteiger et al., 2003) and aligned with the *Torpedo marmorata* α1 subunit sequence using CLUSTALW (http://www.ebi.ac.uk/clustalw) (Thompson et al., 1994). Structural models of the whole hα7 AChR were built applying homology modeling methods using the structure of the *Torpedo* AChR (PDB 2BG9; Unwin, 2005) as template. Modeller 9.14 was used to obtain 100 homology models for each template, and subsequently, their Discrete Optimized Protein Energy profiles (Eswar et al., 2006) were assessed. The best model of each template was subjected to model quality assessment by using the web-based tools of Verify3D (Bowie et al., 1991) and ProCheck (Laskowski et al., 1993).

For the molecular docking procedure, PAM-2 was first built using the semiempirical AM1 method included in Spartan 10 V1.1.0 (Wavefunction, Inc. Irvine, CA 92612 USA). AutoDock Vina (Trott and Olson, 2010) was used for docking simulations of the flexible ligand into the ECD or TMD (including ECD-TMD junction) of the whole, rigid, hα7 AChR and m5-HT_{3A}R (PDB 4PIR; Hassaine et al., 2014) models, respectively. The energetically lower poses were selected from each cluster of superposed poses as described previously (Arias et al., 2013a).

To investigate the stability of the best scored complexes, 15-ns molecular dynamics (MD) simulations were subsequently performed for PAM-2 docked to each binding site at the respective hα7 AChR or m5-HT_{3A}R model, using Desmond v. 3.0.3.1 (Bowers et al., 2006) and OPLS-2005 force field. Each receptor-PAM-2 complex was inserted into 1-palmitoyl-2-oleoyl phosphatidylcholine membranes, and subsequently minimized as described elsewhere (Arias et al., 2015a). Each complex was first minimized and then subjected to 1-ns MD in NVT (constant number of particles, volume, and temperature) ensemble, followed by 15-ns MD in NPT (constant number of particles, pressure, and temperature) ensemble with fixing constrains on protein backbone as previously described (Arias et al., 2015a). Finally, each complex was simulated in NPT ensemble for 15-ns without any fixing constraints. Both NPT and NTV were run with a non-bonded interaction cutoff of 9 Å.

To estimate the stability of the ligand in each binding site, the root-mean-square deviation (RMSD) values were calculated during the 15 ns simulation using the Schrödinger suite software (Schrödinger Release 2015-3: Maestro, v. 10.3). These values represent the intermolecular conformational changes and the translation of the whole molecule in the binding site. The RMSD was calculated using the equation, $\mathrm{RMSD} = \sqrt{\frac{\sum_{i=1}^{N} \delta_i^2}{N}}$, where, N is the number of atoms from the ligand, and δ_i^2 is the distance between the corresponding ligand atoms obtained at each step and the starting conformation. Ligand poses with RMSD values >5 Å were considered unstable and thus were excluded. In addition, the RMSD variance values were calculated during the last 5 ns of the simulation as previously described (Arias et al., 2013b). The poses with the RMSD variance value below 0.5 Å were considered stable (see Supplementary material for the exact values).

2.9. Nonlinear regression analyses

For nonlinear regression analyses of the results obtained from the different experiments previously described, the software Prism 5 (GraphPad Software, Inc., CA, USA) was used.

3. Results

3.1. PAM-2 potentiates hα7 AChRs but not m5-HT_3Rs

The effect of PAM-2 on CH3-hα7 (Fig. 1A) and N1E115-m5-HT_{3A} (Fig. 1B) cells was studied by Ca^{2+} influx assays. Increased concentrations of (±)-epibatidine activate hα7 AChRs (EC_{50} ~52 nM; Table 1). Interestingly, PAM-2 (10 μM) increases the potency (apparent EC_{50} ~17 nM) and efficiency (E_{max} ~190%) of (±)-epibatidine at the hα7 AChR (Table 1). On the other hand, increased concentrations of 5-HT activate m5-HT_{3A}Rs (EC_{50} ~0.55 μM; Fig. 1B). This activation was not enhanced by pre-incubation with PAM-2, but slightly inhibited at very high concentrations of PAM-2 (Table 1).

3.2. Effect of PAM-2 on nicotine-evoked currents in SH-SY5Y cells

The effect of PAM-2 on nicotine (NIC)-evoked AChR currents was studied in SH-SY5Y neuroblastoma cells by using the patch-clamp technique in the whole-cell configuration (Fig. 2). Application of either 10 or 100 μM NIC produces currents of different amplitude and desensitization kinetics (Fig. 2A). Interestingly, NIC-activated currents were not inhibited by 0.1 μM MLA (Fig. 2B). Since MLA is a selective α7 AChR antagonist (Arias et al., 2010), these results suggest that the studied currents are not mediated by α7 AChRs.

Application of increasing concentrations of PAM-2 reduces NIC-evoked currents (Fig. 2A), and the percentage of reduction is the same (87 ± 5% vs 88 ± 5%) when 10 or 100 μM NIC was used to activate AChRs (Fig. 2C). The calculated IC_{50} values indicate that the inhibition is slightly higher when 100 μM NIC was used (Table 1). Interestingly, the effect elicited by NIC, alone or in the presence of PAM-2, was not perturbed by the application of MLA (Fig. 2B). The current reduction by 100 μM PAM-2 is not statistically different in the absence or the presence of MLA ($p > 0.05$), suggesting that this effect is not mediated by α7 AChRs. The observed n_H values (<1; Table 1) indicate that PAM-2 inhibits non-α7 AChRs in a negatively cooperative fashion. This suggests that the inhibitory process is mediated by an allosteric mechanism and not by direct competition with agonist binding, supporting previous results (Arias et al., 2011).

3.3. Effect of PAM-2 on choline-evoked currents in SH-SY5Y-hα7 cells

The activity of PAM-2 was measured in choline-activated SH-SY5Y-hα7 cells by using the patch-clamp technique in the whole-cell configuration. The results indicated that the potentiating activity of PAM-2 was only apparent at low choline concentrations. Indeed, 10 μM PAM-2 enhanced ~50% the current elicited by 100 μM choline, whereas its activity was lost when concentrations ≥1 mM choline were used (Fig. 3A). For this reason the choline concentration dependence of the effect of PAM-2 was analyzed (Fig. 3B). Application of increasing concentrations of PAM-2 potentiates choline-evoked currents with apparent $EC_{50} = 12 \pm 5$ μM ($n_H = 0.74 \pm 0.21$), showing a maximal efficacy $E_{max} = 226 \pm 12\%$ (Fig. 3C).

3.4. Effect of PAM-4 on ACh-activated rα9α10 AChRs

Fig. 4A shows representative responses evoked by 10 μM ACh, corresponding to its EC_{50} value (Elgoyhen et al., 2001) in *X. laevis* oocytes expressing rα9α10 AChRs. Fig. 4B shows representative currents evoked by a subconcentration of ACh ($EC_5 = 1$ μM) either alone or co-applied with a higher concentration of PAM-4 (20 μM). The co-application of 10 μM (Fig. 4A) or 20 μM (Fig. 4B) PAM-4 did not produce a significant effect on the agonist response ($P = 0.99$

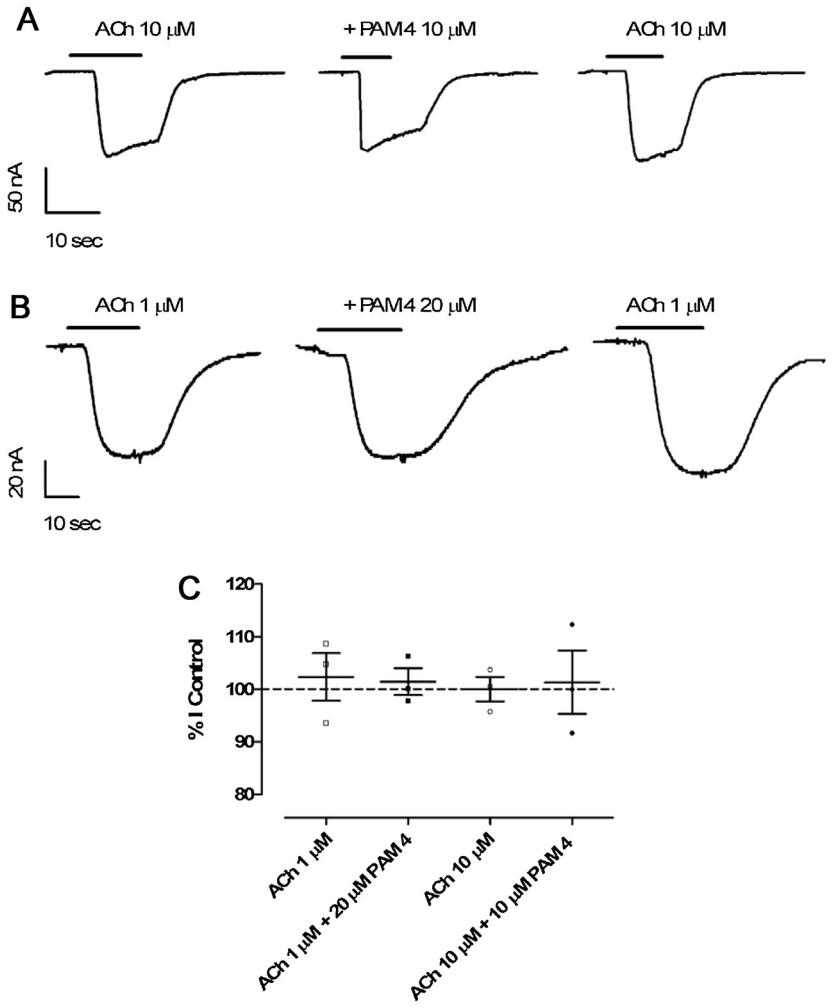

Fig. 4. Effect of PAM-4 on ACh-induced rα9α10 AChR activity. (A) Responses evoked by 10 μM ACh either alone, plus 10 μM PAM-4, or after 3-min wash, in oocytes expressing rα9α10 AChRs (n = 3). (B) Responses evoked by 1 μM ACh either alone, plus 20 μM PAM-4, or after 3-min wash, in oocytes expressing rα9α10 nAChRs (n = 3). (C) Scatter plot displaying the experimental variability of ACh responses, applied alone (n = 3;□, ○) or co-applied with PAM-4 (n = 3; ■, ●). The peak current values are expressed as the percentage of the peak control current elicited by ACh alone (100%). The mean ± SEM for each group is shown in black.

and 0.98, respectively). Fig. 4C shows the variability of the ACh and PAM-4 responses.

3.5. Effect of PAM-2 on different glutamate receptor subtypes

The effect of PAM-2 on NMDA-evoked currents was studied on fibroblasts expressing the hNR1aNR2A and hNR1aNR2B subtypes by using the patch-clamp technique (Fig. 5A). PAM-2 inhibited hNR1aNR2A (81 ± 27 μM) with higher potency than that for hNR1aNR2B (371 ± 77 μM) (Table 1). The n_H value for hNR1aNR2A (0.73 ± 0.20) was close to unity, whereas the n_H value for hNR1aNR2B (0.32 ± 0.03) was lower than unity (Table 1). These results indicate that the observed inhibition is mediated by either a non-cooperative or a negative cooperative mechanism, depending on the receptor subtype.

In the case of AMPARs, 100 μM PAM-2 slightly potentiates Glu-evoked currents in HEK293 cells expressing GluR1 or GluR2 by 45 ± 15% and 123 ± 44%, respectively. Interestingly, the effect elicited by 100 μM PAM-2 is higher than that elicited by 10 μM PAM-2 in the GluR2 ($P < 0.05$) but not in the GluR1 ($P > 0.05$).

Since preliminary results suggest that PAM-2 is inactive on GluR5/K2 receptors, no further experiments were performed on this KA receptor.

3.6. Effect of PAM-2–4 on $Na_v1.2$ and $K_v3.1$ channels

All three PAMs were tested on $Na_v1.2$ and $K_v3.1$ channels using whole-cell patch-clamp. While 100 μM PAM-2–4 only showed minimal blocking effects on $Na_v1.2$ channels (17 ± 15%, 7 ± 2%, and 12 ± 1%, respectively), they were slightly more effective in blocking $K_v3.1$ channels, showing equivalent blockade percentage at the same concentration (51 ± 16%, 60 ± 13%, and 58 ± 5%) (Fig. 6; Table 1). The observed $K_v3.1$ channel inhibition was more clearly concentration-dependent compared to that for $Na_v1.2$.

3.7. Effect of PAM-2 on AChE activity

The Michaelis-Menten kinetics curves show that the AChE reaction rate in the absence of PAM-2 is similar to that obtained in the presence of 100 μM PAM-2 (Fig. 7). The calculated K_m value for the *E. electricus* AChE (167 ± 3 μM ACTh) is in agreement with data reported in the literature (Pastorin et al., 2006; Xu et al., 2008). There was no observable decrease in the V_{max} value (3.02 ± 0.07 nmol/min; $P = 0.284$), indicating that PAM-2 inhibits AChE activity neither in a competitive nor noncompetitive manner.

Table 1
Pharmacologic activity of PAMs on several potential targets.

Molecular Target	Method	Ligand (maximal used concentration)	Pharmacologic activity	Efficacy (E_{max}) or Inhibition (%)	IC_{50} or EC_{50} [c] or K_i [d] (μM)	n_H
hα7 AChR	Ca^{2+} influx	(±)-Epibatidine	Potentiation	100	52 ± 4 nM	3.69 ± 0.06
		(±)-Epibatidine + PAM-2 (10 μM)		190 ± 5	17 ± 5 nM	1.95 ± 0.06
hα7 AChR	Patch-clamp	PAM-2	Potentiation	226 ± 12	12 ± 5[c]	0.74 ± 0.21
hα3-containing AChRs	Patch-clamp	PAM-2	Inhibition	–	13 ± 6[a]	0.52 ± 0.13[a]
					6 ± 5[b]	0.39 ± 0.15[b]
m5-HT_{3A}R	Ca^{2+} influx	PAM-2 (100 μM)	Partial inhibition	–	>100	–
rα9α10 AChR	Voltage-clamp	PAM-4 (20 μM)	None	–	–	–
hNR1aNR2B	Patch-clamp	PAM-2	Inhibition	–	83 ± 27	0.73 ± 0.20
hNR1aNR2A	Patch-clamp	PAM-2	Inhibition	–	371 ± 77	0.32 ± 0.03
GluR5/KA2	Patch-clamp	PAM-2 (100 μM)	No effect	–	–	–
GluR1	Patch-clamp	PAM-2 (100 μM)	Weak potentiation	45 ± 15	–	–
GluR2	Patch-clamp	PAM-2 (100 μM)	Weak potentiation	123 ± 44	–	–
AChE	Enzymatic activity	PAM-2 (100 μM)	None	–	–	–
$Na_v1.2$	Patch-clamp	PAM-2	Partial inhibition	17 ± 15[c]	>100	–
		PAM-3		7 ± 2[c]		
		PAM-4 (100 μM)		12 ± 1[c]		
$K_v3.1$	Patch-clamp	PAM-2	Partial inhibition	51 ± 16[c]	>100	–
		PAM-3		60 ± 13[c]		
		PAM-4 (100 μM)		58 ± 5[c]		
$A_{β42}$ (brain of 5XFAD trangenic mice)	ELISA	PAM-2 (2 mg/kg)	No effect	–	–	–

PAM-2 inhibited hα3-containing AChRs with similar potency using 10 μM[a] or 100 μM[b] nicotine (Fig. 2). [c] PAM-2–4 slightly inhibited $Na_v1.2$ and $K_v3.1$ channels.

Fig. 5. PAM-2 activity at recombinant GluR subtypes. (A) Concentration-response curves for PAM-2 on NR1aNR2A (○) and NR1aNR2B (●) receptors activated by 100 μM NMDA and 10 μM Gly. Each data point is the mean ± SEM (n = 4-7 cells). The obtained r^2 values are 0.99 (○) and 0.95 (●). The calculated IC_{50} and n_H values are summarized in Table 1. (B) Histogram showing the potentiation (% control) elicited by 10 (light bars) and 100 μM (grey bars) PAM-2 on KA (100 μM)-evoked currents in HEK293 cells expressing the GluR1 or GluR2 AMPAR subtype. Each data point is the mean ± SEM (n = 4-8 cells). Student *t*-test analysis indicated that the effect elicited by 100 μM PAM-2 is higher than that elicited by 10 μM PAM-2 in the GluR2 ($P < 0.05$) but not in the GluR1 ($P > 0.05$).

3.8. Effect of PAM-2 on β-amyloid content

To examine whether PAM-2 potentially affects Aβ production which is closely correlated with plaque deposition, brain levels of $A_{β42}$ were determined in 5XFAD mice chronically treated with 2 mg/kg PAM-2. Confirming previous observations (Bhattacharya et al., 2014), $A_{β42}$ concentrations were different between male (3.53 ± 0.29 μg/mL) and female (4.88 ± 0.29 μg/mL) mice irrespective of the treatment (ANOVA, $F_{(1,23)} = 9.369$; $P = 0.005$) (Fig. 8). However, PAM-2 treatment did not significantly affect the $A_{β42}$ concentration (4.53 ± 0.244 μg/mL) when compared to vehicle (4.26 ± 0.40 μg/mL) (ANOVA; females: $F_{(1,15)} = 0.897$, $P = 0.359$; males: $F_{(1,8)} = 1.377$, $P = 0.274$).

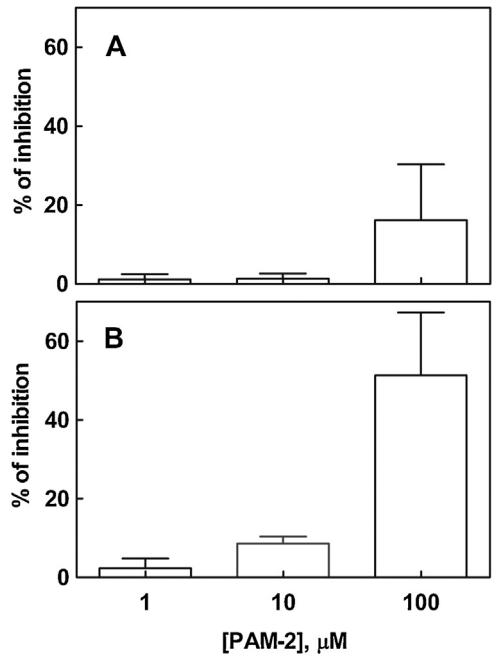

Fig. 6. Effect of PAM-2 on the activity of $Na_v1.2$ (A) and $K_v3.1$ (B) voltage-gated ion channels. Whole-cell patch-clamp experiments (n = 4) were performed as follows: (A) $Na_v1.2$ currents were recorded with 20-ms pulses from −90 mV to 0 mV every 10 s, and (B) $K_v3.1$ currents were elicited by 200-ms depolarizing pulses to 40 mV applied every 10 s. To determine the activity of PAM-2, the current area was determined in the absence and in the presence of 1, 10, and 100 μM PAM-2, respectively, and the percentage of inhibition was calculated. Similar experiments were performed for PAM-3 and PAM-4 (not shown). The inhibition (% control) elicited by each PAM at 100 μM is included in Table 1.

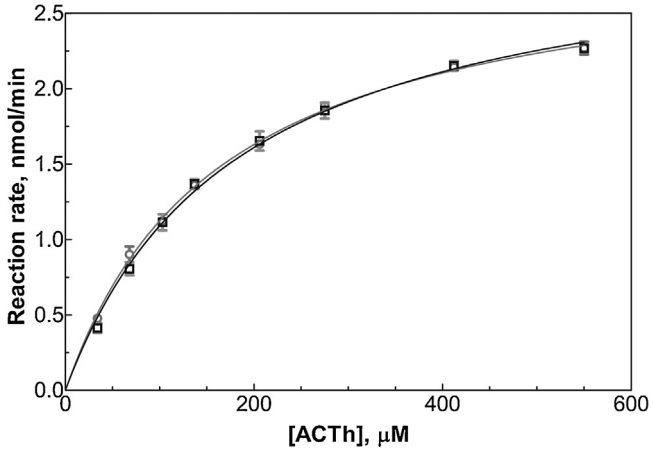

Fig. 7. Michaelis-Menten saturation curves of the hydrolysis of acetylthiocholine (ACTh) by *E. electrophorus* AChE in the absence (○) and presence of 100 μM PAM-2 (□). Student *t*-test analysis revealed no significant differences in the K_m (P = 0.219) and V_{max} (P = 0.284) parameters between control and PAM-2 treatment. These parameters were calculated by fitting the experimental data into the Michaelis-Menten kinetics model.

3.9. Molecular docking and molecular dynamics of PAM-2 at the hα7 AChR and m5-HT_{3A}R models

PAM-2 was docked into the ECD or TMD (including ECD-TMD junction) from each hα7 AChR and m5-HT_{3A}R model (Fig. 9). The docking results using the hα7 AChR model indicate that PAM-2 interacts with allosteric binding sites located at the ECD, ECD-TMD junction, and TMD, whereas it only interacts with the ECD and ECD-TMD junction at the m5-HT_{3A}R model (Fig. 9A; Table 2). The ECD site at the hα7 model is located at the inner β-sheet of the

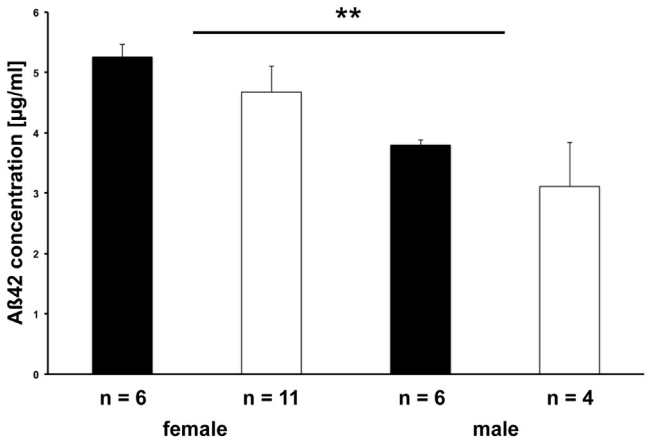

Fig. 8. Effect of PAM-2 on the brain content of $A_{β42}$ in male and female 5XFAD mice. $A_{β42}$ concentrations were determined by ELISA as described in Section 2. Female 5XFAD mice show significantly higher $A_{β42}$ levels than male littermates (ANOVA; $F_{(1,23)} = 9.369$; P = 0.005), irrespective of the treatment. Chronic treatment (26 consecutive days) with 2 mg/kg PAM-2 (black bars) did not significantly affect the $A_{β42}$ concentration compared to vehicle treated controls (white bars) (ANOVA; females: $F_{(1,15)} = 0.897$, P = 0.359; males: $F_{(1,8)} = 1.377$, P = 0.274). ** indicates P < 0.01.

α7/α7 interface as shown previously (Arias et al., 2011). However, in the m5-HT_{3A} model, PAM-2 interacts with the orthosteric site at residues from the principal (i.e., Asn101, Thr154, Trp156, Phe199, Tyr207) and complementary (i.e., Ile44, Arg65, Trp63, Tyr126, and Ile180) components. Since this interaction is not allosteric, it was not included in Fig. 9.

In the hα7 model, PAM-2 also binds to the ECD-TMD junctional site by van der Waals contacts with residues located at the β-strand 10 (first portion; i.e., Arg206 and Arg207), β8–β9 loop (i.e., Glu173), Cys loop (i.e., Phe135), pre-M1 segment (i.e., Thr208, Tyr210, and Tyr211), M2-M3 loop (i.e., Val268, Leu270, and Tyr274), and M2 (i.e., Met261, Thr264 and Phe275) (Fig. 9B, Table 2). Moreover, two hydrogen bonds are formed between the carbonyl oxygen from PAM-2 and the amino moiety of Arg207 (at β-strand 10), as well as between the amino group from PAM-2 and the Thr208 backbone carbonyl (at pre-M1) (Fig. 9B). The calculated RMSD variance value of ~0.03 Å (see Fig. S1A legend; Supplementary material) suggests that the interaction at this site is stable. Although the docking results suggest other two PAM-2 orientations within this junctional site, the MD shows that the molecule departs from its original positions (Fig. S1A; Supplementary material). In the m5-HT_{3A}R, PAM-2 interacts with the ECD-TMD junctional site mainly by van der Waals contacts with residues located at the Cys-loop (i.e., Pro143 and Phe144), pre-M1 segment (i.e., Tyr223, Ala224, and Leu227), M3 (i.e., Ile283 and Phe287), and M4 (i.e., Leu446, Val447, Ile449, and Trp450, Trp453) (Fig. 9B). This site overlaps the site shown in the hα7 models (Fig. 9A; Table 2). The calculated RMSD variance value of ~0.02 Å (see Fig. S2 legend; Supplementary material) suggests that the interaction at this site is stable.

PAM-2 also binds to an intersubunit site in the hα7 model but not in the m5-HT_{3A}R (Table 2). In particular, the ligand intercalates between two α7-TMDs where it interacts with residues located at luminal and non-luminal environments. In particular, PAM-2 interacts mainly by van der Waals contacts with residues at M2 [i.e., Leu255 (position 16′), Ala258 (position 19′), Glu259 (position 20′)] and M3 (i.e., Phe275, Val282, and Val286) from one α7 subunit, and at M1 (i.e., Asn214, Pro218 and Leu221) and M2 [i.e., Leu256 (position 17′), Val257 (position 18′)] from an adjacent α7 subunit. In addition, a hydrogen bond is formed between the amino moiety of Asn214 (at pre-M1) and the carbonyl group of PAM-2. The calculated RMSD variance value of ~0.04 Å (see Fig. S1B legend;

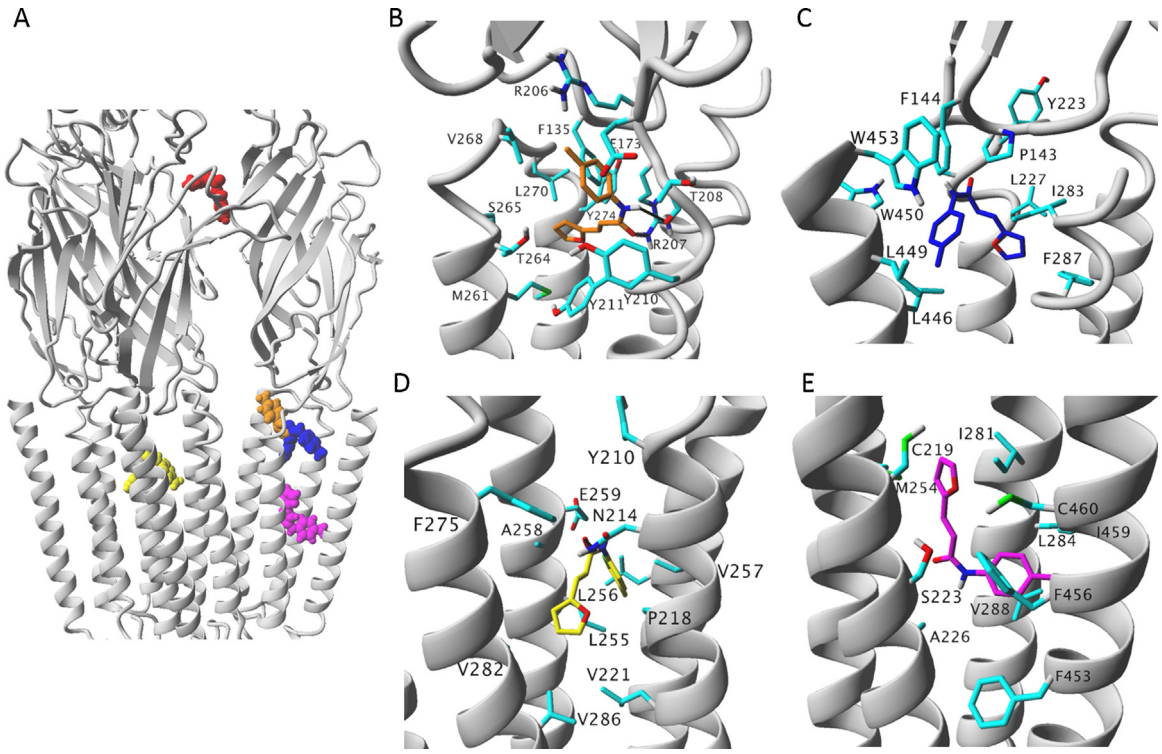

Fig. 9. Molecular docking of PAM-2 to the respective hα7 AChR and m5-HT_{3A}R models. (A) Overlapping of the hα7 AChR and m5-HT_{3A}R models showing the interaction of PAM-2 with the ECD (red), ECD-TMD junction (orange), and TMD [i.e., intersubunit (yellow) and intrasubunit (magenta)] from the hα7 AChR, as well as its interaction with the ECD-TMD junction (blue) at the m5-HT_{3A}R. For clarity, one α7/5-HT_{3A} subunit is hidden. The PAM-2 site at the hα7-ECD (red) has been already described (Arias et al., 2011). (B) In the hα7 AChR, PAM-2 interacts with the ECD-TMD junctional site (orange), mainly by van der Waals contacts with residues located at the β – strand 10 (first portion; Arg206 and Arg207), β8-β9 loop (i.e., Glu173), Cys loop (i.e., Phe135), pre-M1 segment (i.e., Thr208, Tyr210, and Tyr211), M2-M3 loop (i.e., Val268, Leu270, and Tyr274), and M2 (i.e., Met261, Thr264, and Phe275). The black arrows indicate two hydrogen bonds that are formed between the carbonyl oxygen from PAM-2 and the amino moiety of Arg207 (β – strand 10), as well as between the amino group from PAM-2 and the Thr208 backbone carbonyl (pre-M1). (C) In the m5-HT_{3A}R, PAM-2 interacts with the ECD-TMD junction at a site (blue) different to that observed in the hα7 AChR [see (B)] however there is a partial overlapping. More specifically, PAM-2 interacts mainly by van der Waals contacts with residues located at the Cys-loop (i.e., Pro143 and Phe144), pre-M1 segment (i.e., Tyr223, Ala224, and Leu227), M2-M3 loop (i.e., Ile283 and Phe287), and M4 (i.e., Leu446, Val447, Ile449, and Trp450, Trp453). (D) In the intersubunit site (yellow), PAM-2 interacts mainly by van der Waals contacts with residues at M2 [i.e., Leu255, Ala258, Glu259 (20′)] and M3 (i.e., Phe275, Val282, and Val286) from one α7 subunit, and at M1 (i.e., Asn214, Pro218 and Leu221) and M2 [i.e., Leu256 (17′), Val257] from an adjacent α7 subunit. (E) In the intrasubunit site (magenta), PAM-2 interacts with residues at M1 (i.e., Cys219, Ser223, Ala226), M2 (i.e., Met254), M3 (i.e., Ile281, Leu284, and Val288), and M4 (i.e., Phe453, Phe456, Ile459, and Cys460). PAM-2 is rendered in ball (A) or stick (B-E) mode, whereas residues as stick mode (element color code). All non-polar hydrogen atoms are hidden. (For interpretation of the references to colour in this figure legend, the reader is referred to the web version of this article.).

Table 2
Molecular interactions of PAM-2 with allosteric sites at the hα7 AChR and m5-HT_{3A}R models.

Receptor type	Binding site	Residues involved in PAM-2 binding				
		ECD	TM1	TM2 (ring position)	TM3	TM4
hα7 AChR	ECD-TMD junction	Arg206 Arg207 Glu173 Phe135	Thr208 Tyr210 Tyr211	Met261 Thr264 Phe275 Val268 Leu270 Tyr274		
	Intersubunit		Asn214 Pro218 Leu221	Leu255 Leu256 (17′) Val257 Ala258 Glu259 (20′)	Phe275 Val282 Val286	
	Intrasubunit		Cys219 Ser223 Ala226	Met254	Ile281 Leu284 Val288	Phe453 Phe456 Ile459 Cys460
m5-HT_{3A}R	ECD-TMD junction	Phe143 Phe144	Tyr223 Ala224 Leu227		Ile283 Phe287	Val447 Leu446 Leu449 Trp450 Trp453

Supplementary material) suggests that the interaction at this site is stable.

Although initial docking results suggested a luminal site for PAM-2, the MD results indicate that this interaction was unstable during the 15-ns simulation (Fig. S1C; Supplementary material), and thus, it was not included in Fig. 9.

Finally, PAM-2 binds to an intrasubunit site in the hα7 model but not in the m5-HT_{3A}R. The ligand interacts mainly by van der Waals contacts with residues at M1 (Leu216, Cys219, Val220, Ser223, Ala226), M3 (Tyr274, Phe275, Ser277, Thr278, Ile280, Ile281), and M4 (Phe456, Cys460, Thr461, Ile464, Leu465) (Fig. 9E; Table 2). The calculated RMSD variance value of ~0.03 Å (see Fig. S1A legend; Supplementary material) suggests that the interaction at this site is stable.

4. Discussion

The present study shows that PAM-2 is selective for the hα7 AChR, whereas it does not produce important changes in the activity of other ligand- and voltage-gated ion channels, AChE, and in βA_{42} content.

The patch-clamp results obtained using the SH-SY5H cells show that PAM-2 inhibits NIC-evoked currents produced by the activation of endogenous AChR subtypes. These cells express hα3β2, hα3β4, and hα7 AChRs (Dunckley and Lukas, 2006). Considering that the currents were not perturbed by MLA, and that PAM-2 only enhances the activity of hα7 AChRs (Arias et al., 2011), which is not observed in these experiments, we conclude that the detected currents are not provided by hα7 AChRs but by hα3β2 and/or hα3β4 AChRs (i.e., hα3-containing AChRs). The fact that the calculated IC_{50} values (26 and 27 μM) are in the same concentration range as that previously determined for hα3β4 AChRs (12 ± 2 μM) (Arias et al., 2011), supports this notion. The experimental evidence that the calculated inhibitory potency and efficacy of PAM-2 is practically the same when 10 or 100 μM NIC is used to activate hα3-containing AChRs, supports a noncompetitive mechanism of action for PAM-2, which is in agreement with previous results (Arias et al., 2011, 2015a). In addition, PAM-4, which has similar enhancement potency as that for PAM-2 (Arias et al., 2011), produces no changes on the agonist-elicited rα9α10 AChR activity, indicating that this receptor subtype is not essential for its PAM activity.

The patch-clamp results using SH-SY5H-hα7 cells indicated that the higher the used choline concentration, the lower the apparent activity of PAM-2 is observed. A potential explanation for this concentration dependence is that PAM-2 prolongs the opening of the ion channel (the mean open time is increased 7-fold; Andersen et al., 2016), and consequently, the chance of choline molecules blocking the ion channel increases at higher choline concentrations, especially considering that choline is positively charged and that the used membrane potential is −60 mV. Our results concur with Kalappa and Uteshev (2013) studies with PNU-120596, indicating that the activity of type II PAMs could be more apparent at lower agonist concentrations. The determined enhancement potency (~12 μM) for PAM-2 is slightly lower than that previously determined by Ca^{2+} influx (~5 μM), whereas the observed efficacy (~226%) is in the same range as previous determinations (Arias et al., 2011).

The patch-clamp experiments performed on various recombinant GluR subtypes showed that PAM-2 inhibits the NR1aNR2A and NR1aNR2B NMDAR subtypes with low potency. Interestingly, PAM-2 slightly enhances Glu-activated GluR1 and GluR2 AMPAR subtypes, whereas it does not affect the GluR5/K2, a KAR subtype. NMDAR and AMPARs are important for learning and memory processes, including long-term potentiation, and consequently the modulation of these receptors has been targeted to treat several neurological diseases (Gécz, 2010; Collingridge et al., 2013). The observed weak NMDAR inhibition and weak AMPAR potentiation elicited by PAM-2 cannot account for the observed procognitive (Potasiewicz et al., 2015) and promnesic (Targowska-Duda et al., 2016) activities. These results suggest that GluRs are not the targets for the beneficial effects elicited by PAM-2, and that PAM-2 will not produce potential cytotoxic effects mediated by overstimulation of the AMPAR activity.

The patch-clamp results on $Na_v1.2$ and $K_v3.1$ indicated that PAM-2–4 slightly inhibit their activities. Since this inhibition is produced at non-clinically relevant concentrations, it is unlikely that $Na_v1.2$ and $K_v3.1$ expressed in the hippocampus (Ahn et al., 2007; Perney et al., 1992) might mediate the beneficial effects elicited by these PAMs.

The enzymatic studies showed that PAM-2 affect neither the activity of the AChE nor $A_{\beta42}$ content in transgenic mice. These results support the view that the procognitive (Potasiewicz et al., 2015) and promnesic (Targowska-Duda et al., 2016) activity elicited by PAM-2 is not consequence of an increased synaptic ACh concentration or a reduced plaque formation by an increased degradation or diminished synthesis of $A_{\beta42}$. In this regard, PAM-induced α7 AChR potentiation opens the possibility for novel therapies for the treatment of Alzheimer's disease based on different mechanisms compared to the current medications grounded on AChE inhibition or to drugs that decrease Aβ content (Vassar, 2014).

The Ca^{2+} influx results show that PAM-2 produces no significant effect on agonist-elicited m5-HT_{3A}R responses. These results correspond very well to the outcome on m5-HT_{3A}Rs using patch-clamp methods (Andersen et al., 2016), supporting the notion that the various behavioral activities elicited by PAM-2 using different animal models are not determined by its action on 5-HT_{3A}Rs.

Based on the experimental evidence that PAM-2 does not affect m5-HT_{3A}Rs (see previous paragraph) but enhances the activity of hα7 AChRs (Arias et al., 2011; Andersen et al., 2016), the molecular interactions of PAM-2 for the hα7 AChR was compared to that for the m5-HT_{3A}R. The results indicated that PAM-2 may interact with different sites located at the ECD, TMD, and ECD-TMD junction. Based on MD studies, we previously suggested that the active site for PAM-2 is located at the hα7-ECD (Arias et al., 2011). However, new evidence indicating that PAM-2 is active neither at the m5-HT_3R (this work) nor at the α7-ECD/5-HT_{3A}-TMD chimera (Andersen et al., 2016) suggests that the hα7-ECD is not involved in the activity of PAM-2. Considering that this chimera also has several structural components from the ECD-TMD junctional domain corresponding to the hα7 AChR (e.g., the M2-M3 loop), this domain could also be excluded as the active site for PAM-2. In this regard, the only two remnant active sites for PAM-2 at the hα7 AChR are the intersubunit and intrasubunit sites.

The intrasubunit site for PAM-2 corresponds to that characterized for PNU-120596, the archetypical type II PAM (Young et al., 2008; daCosta et al., 2011). The structural similitude between the binding sites for PAM-2 and PNU-120596 supports previous functional results where PAM-2 was classified as a type II PAM because it reactivates desensitized α7 AChRs (Targowska-Duda et al., 2014).

The results from this work are in agreement with our original conclusions, indicating that PAM-2–4, are selective PAMs for the α7 AChR (Arias et al., 2011), and consequently, that the antidepressant-like (Targowska-Duda et al., 2014; Arias et al., 2015a,b), procognitive (Potasiewicz et al., 2015), promnesic (Targowska-Duda et al., 2016), and antinociceptive and anti-inflammatory (Bagdas et al., 2015) activities elicited by PAM-2 are mediated by none of the potential targets studied in this work. Finally, the potential binding site for PAM-2 overlaps the intrasubunit site corresponding to that for PNU-120596, the archetypical

type II PAM. Nevertheless, PAM-2 also binds to an intersubunit site, opening the door for additional types of allosteric mechanisms.

Acknowledgements

This research was supported by grants from the Polish National Science Center (Sonata funding, UMO-2013/09/D/NZ7/04549) [to K.T-D. (PI) and H.R.A. (Co-PI)]. Calculations were partially performed under a computational grant G30-18) by the Interdisciplinary Center for Mathematical and Computational Modeling (ICM), Warsaw, Poland, and under resources and licenses from CSC, Finland (to A.K). B.M.B. was supported by a National Heart, Lung & Blood Institute T32 Training Program in Basic and Translational Cardiovascular Science [T32HL086350]. We gratefully acknowledge the technical assistance of Daniela Hill and Karla Sowa at Dr. Montag's lab.

Appendix A. Supplementary data

Supplementary data associated with this article can be found, in the online version, at http://dx.doi.org/10.1016/j.biocel.2016.04.015.

References

Ahn, M., Beacham, D., Westenbroek, R.E., Scheuer, T., Catterall, W.A., 2007. Regulation of $Na_V1.2$ channels by brain-derived neurotrophic factor, TrkB, and associated Fyn kinase. J. Neurosci 27, 11533–11542.

Andersen, N.D., Nielsen, B.E., Corradi, J., Tolosa, M.F., Feuerbach, D., Arias, H.R., et al., 2016. Exploring the positive allosteric modulation of human α7 nicotinic receptors from a single-channel perspective. Neuropharmacology 107, 189–200.

Arias, H.R., Gu, H., Feuerbach, D., Wei, D.-Q., 2010. Different interaction between the agonist JN403 and the competitive antagonist methyllycaconitine with the human α7 nicotinic receptor. Biochemistry 49, 4169–4180.

Arias, H.R., Gu, R.X., Feuerbach, D., Guo, B.B., Ye, Y., Wei, D.Q., 2011. Novel positive allosteric modulators of the human α7 nicotinic acetylcholine receptor. Biochemistry 50, 5263–5278.

Arias, H.R., Targowska-Duda, K.M., Feuerbach, D., Jozwiak, K., 2013a. Mecamylamine inhibits muscle nicotinic acetylcholine receptors by competitive and noncompetitive mechanisms. OA Biochemistry 1, 7.

Arias, H.R., López, J.J., Feuerbach, D., Fierro, A., Ortells, M.O., Pérez, E.G., 2013b. Novel 2-(substituted benzyl)quinuclidines inhibit human α7 and α4β2 nicotinic receptors by different mechanisms. Int. J. Biochem. Cell Biol. 45, 2420–2430.

Arias, H.R., Feuerbach, D., Targowska-Duda, K., Kaczor, A.A., Poso, A., Jozwiak, K., 2015a. Pharmacological and molecular studies on the interaction of varenicline with different nicotinic acetylcholine receptor subtypes. Potential mechanism underlying partial agonism at human α4β2 and α3β4 subtypes. Biochim. Biophys. Acta 1884, 731–741.

Arias, H.R., Targowska-Duda, K.M., Feuerbach, D., Jozwiak, K., 2015b. The antidepressant-like activity of nicotine, but not of 3-furan-2-yl-*N*-p-tolyl-acrylamide, is regulated by the nicotinic receptor β4 subunit. Neurochem. Int. 87, 110–116.

Arias, H.R., 2010. Positive and negative modulation of nicotinic receptors. Adv. Protein Chem. Struct. Biol. 80, 153–203.

Arias, H.R., 2011. Allosteric modulation of nicotinic acetylcholine receptors. In: Arias, H.R. (Ed.), Pharmacology of Nicotinic Acetylcholine Receptors from the Basic and Therapeutic Perspectives. Research Signpost, Kerala, India, pp. 51–173 (Chapter 7).

Bagdas, D., Targowska-Duda, K.M., Lopez, J.J., Perez, E.G., Arias, H.R., Damaj, M.I., 2015. Antinociceptive and anti-inflammatory properties of 3-furan-2-yl-*N*-*p*-tolyl-acrylamide (PAM-2) a positive allosteric modulator of α7 nicotinic acetylcholine receptors, in mice. Anesth. Analg. 121, 1369–1377.

Bhattacharya, S., Haertel, C., Maelicke, A., Montag, D., 2014. Galantamine slows down plaque formation and behavioral decline in the 5XFAD mouse model of Alzheimer's disease. PLoS One 9, e89454.

Bowers, K.J., Chow, E., Xu, H., Dror, R.O., Eastwood, M.P., Gregersen, B.A., et al., 2006. Algorithms for molecular dynamics simulations on commodity clusters. D. E. shaw research, LLC, new York, NY 10036, USA. In: Proceedings of the ACM/IEEE Conference on Supercomputing (SC06), November 11–17, Tampa Florida.

Bowie, J.U., Luthy, R., Eisenberg, D., 1991. A method to identify protein sequences that fold into a known three-dimensional structure. Science 253, 164–170.

Chatzidaki, A., Millar, N.S., 2015. Allosteric modulation of nicotinic acetylcholine receptors. Biochem. Pharmacol. 97, 408–417.

Collingridge, G.L., Volianskis, A., Bannister, N., France, G., Hanna, L., Mercier, M., et al., 2013. The NMDA receptor as a target for cognitive enhancement. Neuropharmacology 64, 13–26.

daCosta, C.J., Free, C.R., Corradi, J., Bouzat, C., Sine, S.M., 2011. Single-channel and structural foundations of neuronal α7 acetylcholine receptor potentiation. J. Neurosci. 31, 13870–13879.

Dunckley, T., Lukas, R.J., 2006. Nicotinic modulation of gene expression in SH-SY5Y neuroblastoma cells. Brain Res. 1116, 39–49.

Elgoyhen, A.B., Vetter, D.E., Katz, E., Rothlin, C.V., Heinemann, S.F., 2001. Alpha10: a determinant of nicotinic cholinergic receptor function in mammalian vestibular and cochlear mechanosensory hair cells. Proc. Natl. Acad. Sci. U. S. A. 98, 3501–3506.

Ellman, G.L., Courtney, K.D., Featherstone, R.M., 1961. A new and rapid colorimetric determination of acetylcholinesterase activity. Biochem. Pharmacol. 7, 88–95.

Eswar, N., Webb, B., Marti-Renom, M.A., Madhusudhan, M.S., Eramian, D., Shen M.Y. et al., 2006. Comparative protein structure modeling using Modeller., Curr. Protoc. Bioinformatics John Wiley & Sons, Inc., Suppl. 15, 5.6. 1–5.6.30.

Gécz, J., 2010. Glutamate receptors and learning and memory. Nat. Genet. 42, 925–926.

Gasteiger, E., Gattiker, A., Hoogland, C., Ivanyi, I., Appel, R.D., Bairoch, A., 2003. ExPASy: the proteomics server for in-depth protein knowledge and analysis. Nucl. Acids Res. 31, 3784–3788.

Grissmer, S., Nguyen, A.N., Aiyar, J., Hanson, D.C., Gutman, G.A., Mather, R.J., et al., 1994. Pharmacological characterization of five cloned voltage-gated K^+ channels, types $K_V1.1$, 1.2, 1.3, 1.5, and 3.1, stably expressed in mammalian cell lines. Mol. Pharmacol. 45, 1227–1234.

Hassaine, G., Deluz, C., Grasso, L., Wyss, R., Tol, M.B., Hovius, R., et al., 2014. X-ray structure of the mouse serotonin 5-HT_3 receptor. Nature 512, 276–281.

Hussy, N., Lukas, W., Jones, K.A., 1994. Functional properties of a cloned 5-hydroxytryptamine ionotropic receptor subunit: comparison with native mouse receptors. J. Physiol. 481, 311–323.

Kalappa, B.I., Uteshev, V.V., 2013. The dual effect of PNU-120596 on α_7 nicotinic acetylcholine receptor channels. Eur. J. Pharmacol. 718, 226–234.

Laskowski, R.A., MacArthur, M.W., Moss, D.S., Thornton, J.M., 1993. PROCHECK—a program to check the stereochemical quality of protein structures. J. Appl. Crystallogr. 26, 283–291.

Losi, G., Garzon, G., Puia, G., 2008. Nongenomic regulation of glutamatergic neurotransmission in hippocampus by thyroid hormones. Neuroscience 151, 155–163.

Malysz, J., Grønlien, J.H., Timmermann, D.B., Håkerud, M., Thorin-Hagene, K., Ween, H., et al., 2009. Evaluation of α7 nicotinic acetylcholine receptor agonists and allosteric modulators using the parallel oocyte electrophysiology test station. Assay Drug Dev. Technol. 7, 374e390.

Oakley, H., Cole, S.L., Logan, S., Maus, E., Shao, P., Craft, J., Guillozet-Bongaarts, A., Ohno, M., Disterhoft, J., Van Eldik, L., Berry, R., Vassar, R., 2006. Intraneuronal β-amyloid aggregates, neurodegeneration, and neuron loss in transgenic mice with five familial Alzheimer's disease mutations: potential factors in amyloid plaque formation. J. Neurosci. 26, 10129–10140.

Perney, T.M., Marshall, J., Martin, K.A., Hockfield, S., Kaczmarek, L.K., 1992. Expression of the mRNAs for the Kv3. 1 potassium channel gene in the adult and developing rat brain. J. Neurophysiol. 68, 756–766.

Pastorin, G., Marchesan, S., Hoebeke, J., Da Ros, T., Ehret-Sabatier, L., Briand, J.P., Prato, M., Bianco, A., 2006. Design and activity of cationic fullerene derivatives as inhibitors of acetylcholinesterase. Org. Biomol. Chem. 4, 2556–2562.

Potasiewicz, A., Kos, T., Ravazzini, F., Puia, G., Arias, H.R., Popik, P., et al., 2015. Pro-cognitive activity in rats of 3-furan-2-yl-*N*-*p*-tolyl-acrylamide, a positive allosteric modulator of the α7 nicotinic acetylcholine receptor. Br. J. Pharmacol. 172, 5123–5135.

Schmitz, A., Sankaranarayanan, A., Azam, P., Schmidt-Lassen, K., Homerick, D., 2005. Design of PAP-1 a selective small molecule $K_V1.3$ blocker, for the suppression of effector memory T cells in autoimmune diseases. Mol. Pharmacol. 68, 1254–1270.

Storch, A., Schrattenholz, A., Cooper, J.C., Abdel Ghani, E.M., Gutbrod, O., 1995. Physostigmine, galanthamine and codeine act as 'noncompetitive nicotinic receptor agonists' on clonal rat pheochromocytoma cells. Eur. J. Pharmacol. 290, 207–219.

Targowska-Duda, K.M., Feuerbach, D., Biała, G., Jozwiak, K., Arias, H.R., 2014. Antidepressant activity in mice elicited by 3-furan-2-yl-N-p-tolyl-acrylamide, a positive allosteric modulator of the α7 nicotinic receptor. Neurosci. Lett. 569, 126–130.

Targowska-Duda, K.M., Wnorowski, A., Budzynska, B., Jozwiak, K., Biała, G., Arias, H.R., 2016. The positive allosteric modulator of α7 nicotinic acetylcholine receptors, 3-furan-2-yl-*N*-*p*-tolyl-acrylamide, enhances memory processes and stimulates ERK1/2 phosphorylation in mice. Behav. Brain Res. 302, 142–151.

Thompson, J.D., Higgins, D.G., Gibson, T.J., 1994. CLUSTAL W: improving the sensitivity of progressive multiple sequence Alignment through sequence weighting, position-specific gap penalties and weight matrix choice. Nucleic Acids Res. 22, 4673–4680.

Trott, O., Olson, A.J., 2010. AutoDock Vina: improving the speed and accuracy of docking with a new scoring function, efficient optimization, and multithreading. J. Comput. Chem. 31, 455–461.

Unwin, N., 2005. Refined structure of the nicotinic acetylcholine receptor at 4A resolution. J. Mol. Biol. 346, 967–989.

Vassar, R., 2014. BACE1 inhibitor drugs in clinical trials for Alzheimer's disease. Alzheimer's Res. Ther. 6, 89.

Verbitsky, M., Rothlin, C.V., Katz, E., Elgoyhen, A.B., 2000. Mixed nicotinic-muscarinic properties of the alpha9 nicotinic cholinergic receptor. Neuropharmacology 39, 2515–2524.
Xu, Z., Yao, S., Wei, Y., Zhou, J., Zhang, L., Wang, C., Guo, Y., 2008. Monitoring enzyme reaction and screening of inhibitors of acetylcholinesterase by quantitative matrix-assisted laser desorption/ionization Fourier transform mass spectrometry. J. Am. Soc. Mass Spectrom. 19, 1849–1855.
Young, G.T., Zwart, R., Walker, A.S., Sher, E., Millar, N.S., 2008. Potentiation of α7 nicotinic acetylcholine receptors via an allosteric transmembrane site. Proc. Natl. Acad. Sci. U. S. A. 105, 14686–14691.